Gravitational waves from a dark $U(1)_D$ phase transition in light of NANOGrav 12.5 yr data

Debasish Borah[1,*], Arnab Dasgupta,[2,†] and Sin Kyu Kang[3,‡]

[1]*Department of Physics, Indian Institute of Technology Guwahati, Assam 781039, India*
[2]*Institute of Convergence Fundamental Studies, Seoul-Tech, Seoul 139-743, Korea*
[3]*School of Liberal Arts, Seoul-Tech, Seoul 139-743, Korea*

We study a possibility of a strong first-order phase transition taking place below the electroweak scale in the context of a $U(1)_D$ gauge extension of the standard model. As pointed out recently by the NANOGrav Collaboration, gravitational waves from such a phase transition with appropriate strength and nucleation temperature can explain their 12.5 yr data. We first find the parameter space of this minimal model consistent with NANOGrav findings by considering only a complex singlet scalar and $U(1)_D$ vector boson. The existence of a singlet fermion charged under $U(1)_D$ can give rise to dark matter in this model, preferably of nonthermal type, while incorporating additional fields can also generate light neutrino masses through typical low-scale seesaw mechanisms like a radiative or inverse seesaw.

I. INTRODUCTION

The NANOGrav Collaboration has recently released their results for gravitational-wave (GW) background produced from a first-order phase transition (FOPT) in 45 pulsars from their 12.5 year data [1]. According to their analysis, the 12.5 yr data can be explained in terms of a FOPT occurring at a temperature below the electroweak (EW) scale, although there exists degeneracy with similar signals generated by supermassive black hole binary (SMBHB) mergers. Last year, the same collaboration also reported evidence for a stochastic GW background with a power-law spectrum having frequencies around the nHz regime [2] which led to several interesting new physics explanations; for example, Refs. [3–5] studied cosmic string origins and Refs. [5–9] studied FOPT origins. Pulsar-timing arrays (PTAs) like NANOGrav that are sensitive to GWs of extremely low frequencies offer a complementary probe of the GW background to future space-based interferometers like eLISA [10,11].

Inspired by the results from NANOGrav explained in terms of a FOPT characterized by the preferred ranges for the strength (α_*) and temperature (T_*) of the phase

transition as shown in Ref. [1], we propose a simple model to achieve such a low-scale strong FOPT. For our purpose, we introduce a dark $U(1)_D$ gauge symmetry under which only a complex singlet scalar Φ and a vector-like singlet fermion Ψ are charged, while all of the standard model (SM) particles are neutral. Since the SM particles are neutral under this gauge symmetry, one can evade strong bounds from experiments on the corresponding gauge coupling g_D and gauge boson mass M_{Z_D}. We further impose a classical conformal invariance so that $U(1)_D$ symmetry breaking occurs only via radiative effects on the scalar potential, naturally leading to a vacuum below the EW scale. Then, a strong FOPT can take place at a bubble nucleation temperature much below the electroweak scale. For earlier works on FOPT within such Abelian gauge extended scenarios, please refer to Refs. [12–18] and references therein.

While such a strongly first-order dark phase transition and resulting gravitational waves have been discussed earlier as well, we study this possibility for the first time after the NANOGrav Collaboration analyzed their 12.5 year data in the context of gravitational waves from the FOPT at a low temperature below the EW scale [1]. In addition, we note that the dark $U(1)_D$ symmetry can also be motivated from tiny neutrino masses and dark matter (DM), which the SM fails to address. In this work, we examine how tiny neutrino masses can be generated through a low-scale seesaw mechanism like a radiative or inverse seesaw, and a singlet fermion charged under $U(1)_D$ can be a good dark matter candidate while keeping the model parameters consistent with the results from NANOGrav.

*[*]dborah@iitg.ac.in
[†]arnabdasgupta@protonmail.ch
[‡]skkang@seoultech.ac.kr

II. THE MODEL

As mentioned above, we consider a $U(1)_D$ extension of the SM. The newly introduced fields are a complex scalar Φ and a vector-like fermion Ψ with $U(1)_D$ charges $2n_1$ and n_1, respectively. All of the SM fields are neutral under this new gauge symmetry. The zero-temperature scalar potential at tree level is given by

$$V_{\text{tree}} = \lambda_H |H|^4 + \lambda |\Phi|^4 - \lambda' |\Phi|^2 |H|^2, \qquad (1)$$

where H is the SM Higgs doublet. Note the absence of bare mass squared terms due to the conformal invariance imposed. The vacuum expectation value (VEV) of the singlet scalar, $\langle \Phi \rangle = M/\sqrt{2}$, acquired via the running of the quartic coupling λ breaks the gauge symmetry, leading to a massive gauge boson $M_{Z_D} = 2g_D M$. In order to realize the electroweak vacuum, the coupling λ' needs to be suppressed, so in our analysis we neglect the coupling λ'. We also consider the Yukawa coupling (y) of the scalar singlet with the fermion Ψ to be negligible compared to the gauge coupling, $g_D \gg y$, so as to suppress its role in the renormalization group equation (RGE) of the singlet quartic coupling. Such assumptions are taken for simplicity and also to make sure that the Higgs VEV does not affect the light singlet scalar mass in any possible way.

The total effective potential can be schematically divided into the following form:

$$V_{\text{tot}} = V_{\text{tree}} + V_{\text{CW}} + V_{\text{th}}, \qquad (2)$$

where $V_{\text{tree}}, V_{\text{CW}},$ and V_{th} denote the tree-level scalar potential, the one-loop Coleman-Weinberg potential, and the thermal effective potential, respectively. In finite-temperature field theory, the effective potential, V_{CW}, and V_{thermal} are calculated using the standard back ground field method [19,20]. We consider Landau gauge throughout this work. Issues related to gauge dependence in such conformal models have been discussed recently by the authors of Ref. [18]. Denoting the singlet scalar as $\Phi = (\phi + M + iA)/\sqrt{2}$, the zero-temperature effective potential up to one loop can be written as [12]

$$V_0 = V_{\text{tree}} + V_{\text{CW}}$$
$$= \frac{1}{4} \lambda(t) G^4(t) \phi^4, \qquad (3)$$

where $t = \log(\phi/\mu)$ with μ being the scale of renormalization. $G(t)$ is given by

$$G(t) = e^{-\int_0^t dt' \gamma(t')}, \qquad \gamma(t) = -\frac{a_2}{32\pi^2} g_D^2(t), \qquad (4)$$

where we have ignored ϕ couplings with Ψ as well as the SM Higgs H for simplicity. In the above equation, $a_2 = 24$.

The gauge coupling $g_D(t)$ and quartic coupling $\lambda(t)$ at the renormalization scale can be calculated by solving the corresponding RGEs. In terms of $\alpha_D = g_D^2/4\pi$ and $\alpha_\lambda = \lambda/4\pi$, the RGEs are

$$\frac{d\alpha_D(t)}{dt} = \frac{b}{2\pi} \alpha_D^2(t), \qquad (5)$$

$$\frac{d\alpha_\lambda(t)}{dt} = \frac{1}{2\pi}(a_1 \alpha_\lambda^2(t) + 8\pi \alpha_\lambda(t)\gamma(t) + a_3 \alpha_D^2(t)), \quad (6)$$

where $b = 8/3$, $a_1 = 10$, and $a_3 = 48$. Taking the renormalization scale μ to be M, the condition $\frac{dV}{d\phi}|_{\phi=M} = 0$ leads us to the relation

$$a_1 \alpha_\lambda(0)^2 + a_3 \alpha_D(0)^2 + 8\pi \alpha_\lambda(0) = 0, \qquad (7)$$

which makes $\alpha_\lambda(0)$ determined by $\alpha_D(0)$. Since the running of the coupling can be solved analytically, the scalar potential can be given by [12]

$$V_0(\phi, t) = \frac{\pi \alpha_\lambda(t)}{(1 - \frac{b}{2\pi} \alpha_D(0)t)^{a_2/b}} \phi^4, \qquad (8)$$

where

$$\alpha_D(t) = \frac{\alpha_D(0)}{1 - \frac{b}{2\pi} \alpha_D(0)t}, \qquad (9)$$

$$\alpha_\lambda(t) = \frac{a_2 + b}{2a_1} \alpha_D(t)$$
$$+ \frac{A}{a_1} \alpha_D(t) \tan\left[\frac{A}{b} \ln[\alpha_D(t)/\pi] + C\right],$$
$$A \equiv \sqrt{a_1 a_3 - (a_1 + b)^2/4}, \qquad (10)$$

and the coefficient C is determined by Eq. (7).

Thermal contributions to the effective potential are given by

$$V_{\text{th}} = \sum_i \left(\frac{n_{B_i}}{2\pi^2} T^4 J_B\left[\frac{m_{B_i}}{T}\right] - \frac{n_{F_i}}{2\pi^2} J_F\left[\frac{m_{F_i}}{T}\right]\right), \qquad (11)$$

where n_{B_i} and n_{F_i} denote the degrees of freedom (d.o.f.) of the bosonic and fermionic particles, respectively. In this expression, J_B and J_F are defined as follows:

$$J_B(x) = \int_0^\infty dz\, z^2 \log\left[1 - e^{-\sqrt{z^2+x^2}}\right],$$

$$J_F(x) = \int_0^\infty dz z^2 \log\left[1 + e^{-\sqrt{z^2+x^2}}\right]. \qquad (12)$$

On calculating V_{th}, we include a contribution from the daisy diagram to improve the perturbative expansion during

the phase transition [21–23]. The daisy-improved effective potential can be calculated by inserting thermal masses into the zero-temperature field-dependent masses. The author of Ref. [22] proposed the thermal resummation prescription in which the thermal-corrected field-dependent masses are used for the calculation in V_{CW} and V_{th} (Parwani method). In comparison to this prescription, authors of Ref. [23] proposed an alternative prescription for the thermal resummation (Arnold-Espinosa method). They included the effect of the daisy diagram only for Matsubara zero modes inside the J_B function defined above. In our work, we use the Arnold-Espinosa method. As mentioned before, we ignore the singlet scalar coupling to fermions and the SM Higgs and hence calculate the field-dependent and thermal masses as well as the daisy diagram contribution for the vector boson only.

As the evolution has two scales, ϕ and T, where T is the temperature of the Universe, we consider the renormalization scale parameter u instead of t as

$$u \equiv \log(\Lambda/M) \quad \text{where } \Lambda \equiv \max(\phi, T). \quad (13)$$

Note that Λ represents the typical scale of the theory. Now, the one-loop-level effective potential is given as

$$V_{tot}(\phi, T) = V_0(\phi, u) + V_T(\phi, T), \quad (14)$$

where

$$V_T(\phi, T) = \frac{3}{2} V_T^B(m_V(\phi)/T, T) + V_{daisy}(\phi, T), \quad (15)$$

$$V_T^B(x, T) \equiv \frac{T^4}{\pi^2} \int_0^\infty dz \, z^2 \ln[1 - e^{-\sqrt{z^2+x^2}}],$$

$$V_{daisy}(\phi, T) = -\frac{T}{12\pi}[m_V^3(\phi, T) - m_V^3(\phi)], \quad (16)$$

where V_T^B is the thermal correction and V_{daisy} is the daisy subtraction [21–23].

III. FIRST-ORDER PHASE TRANSITION

The first-order phase transitions proceed via tunneling, and the corresponding spherically symmetric field configurations called bubbles are nucleated, followed by expansion and coalescence.[1] The tunneling rate per unit time per unit volume is given as

$$\Gamma(T) = \mathcal{A}(T)e^{-S_3(T)/T}, \quad (17)$$

where $\mathcal{A}(T) \sim T^4$ and $S_3(T)$ are determined by the dimensional analysis and given by the classical configurations, called bounce, respectively. At finite temperature, the

$O(3)$-symmetric bounce solution [26] is obtained by solving the following equation:

$$\frac{d^2\phi}{dr^2} + \frac{2}{r}\frac{d\phi}{dr} = \frac{\partial V_{tot}}{\partial\phi}. \quad (18)$$

The boundary conditions for the above differential equation are

$$\phi(r \to \infty) = \phi_{false}, \qquad \frac{d\phi}{dr}\bigg|_{r=0} = 0, \quad (19)$$

where ϕ_{false} denotes the position of the false vacuum. Using ϕ governed by the above equation and boundary conditions, the bounce action can be written as

$$S_3 = \int_0^\infty dr 4\pi r^2 \left[\frac{1}{2}\left(\frac{d\phi}{dr}\right)^2 + V_{tot}(\phi, T)\right]. \quad (20)$$

The temperature at which the bubbles are nucleated is called the nucleation temperature T_*. This can be calculated by comparing the tunneling rate to the Hubble expansion rate as

$$\Gamma(T_*) = \mathbf{H}^4(T_*). \quad (21)$$

Here, assuming the usual radiation-dominated Universe, the Hubble parameter is given by $\mathbf{H}(T) \simeq 1.66\sqrt{g_*}T^2/M_{Pl}$, with g_* being the d.o.f. of the radiation component. Thus, the rate comparison equation above leads to

$$\frac{S_3(T_*)}{T_*} \simeq 140, \quad (22)$$

for $g_* \sim 100$ and $T_* \sim 100$ GeV, while for lower temperatures near MeV it comes down to $g_* \sim 10$. If $\phi(T_*)/T_* > 1$ is satisfied, where $\phi(T_*)$ is the singlet scalar VEV at the nucleation temperature, $T = T_*$, the corresponding phase transition is conventionally called *strong* first order.

By choosing the benchmark values $\alpha_* = 0.68$, $T_* = 2.25$ MeV, $g_D = 0.32$, $M_{Z_D} = 12.6$ MeV, we can portray the curves of the potential in terms of ϕ/M at the critical and nucleation temperatures, as shown in Fig. 1. Clearly, we see that $\phi = 0$ becomes a false vacuum below the critical temperature T_c and the existence of the barrier at T_c indicates a strong first-order phase transition driven by the singlet scalar sector, which triggers bubble production and subsequent production of GWs.

The phase transition completes via the percolation of the growing bubbles. To see when the phase transition finishes, we need to estimate the percolation temperature T_p at which a significant volume of the Universe has been converted from the symmetric to the broken phase. Following Refs. [27,28], T_p is obtained from the probability of finding a point still in the false vacuum given by

---

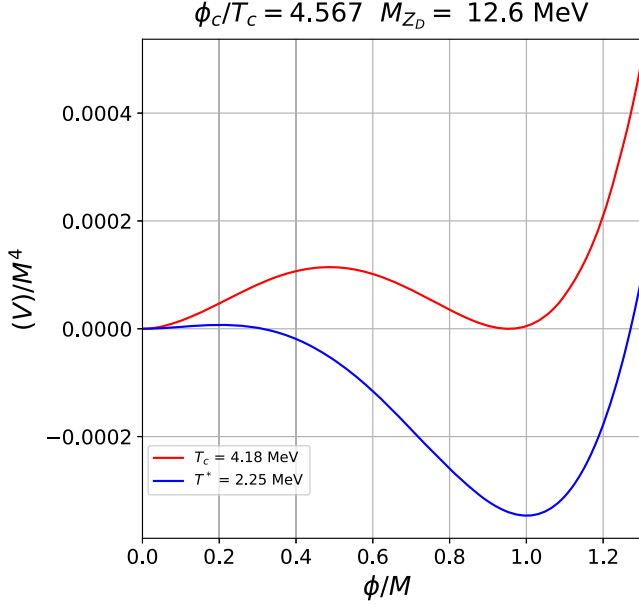[1]For recent reviews of cosmological phase transitions, see Refs. [24,25].

FIG. 1. Shape of the potential at the critical and nucleation temperatures for the chosen benchmark $\alpha_* = 0.68$, $T_* = 2.25$ MeV, $g_D = 0.32$, $M_{Z_D} = 12.6$ MeV.

$$\mathcal{P}(T) = e^{-\mathcal{I}(T)}, \quad \text{where}$$

$$\mathcal{I}(T) = \frac{4\pi}{3} \int_T^{T_c} \frac{dT'}{T'^4} \frac{\Gamma(T')}{\mathbf{H}(T')} \left(\int_T^{T'} \frac{d\tilde{T}}{\mathbf{H}(\tilde{T})} \right)^3. \quad (23)$$

The percolation temperature is then calculated by using $\mathcal{I}(T_p) = 0.34$ [27] (implying that at least 34% of the comoving volume is occupied by the true vacuum). It is also necessarily required that the physical volume of the false vacuum should be decreased around percolation for successful completion of the phase transition. This requirement reads

$$\frac{1}{\mathcal{V}_{\text{false}}} \frac{d\mathcal{V}_{\text{false}}}{dx} = \mathbf{H}(T) \left(3 + T \frac{d\mathcal{I}(T)}{dT} \right) < 0, \quad (24)$$

where x is denoted as time.

Confirming that this condition is satisfied at the percolation temperature T_p, one can ensure that the phase transition successfully completes. For the same benchmark values as those taken in Fig. 1, we calculate the percolation temperature T_p and check that the condition Eq. (24) is satisfied. The results and values of some parameters are presented in Table I.

TABLE I. Numerical values of parameters leading to Fig. 3.

α_*	$(\beta/\mathbf{H}_*)$	T_*	v_w	T_p	$\frac{1}{\mathcal{V}_{\text{false}}} \frac{d\mathcal{V}_{\text{false}}}{dx}$
0.68	82.4	2.25 MeV	0.91	1.9 MeV	-24.17 GeV

IV. GRAVITATIONAL WAVES

As mentioned before, a strong FOPT can lead to the generation of stochastic gravitational-wave signals. In particular, GW signals during such a strong FOPT are generated by bubble collisions [29–33], the sound wave of the plasma [34–37], and the turbulence of the plasma [38–43].

The amplitudes of GWs depend upon the ratio of the amount of vacuum energy released by the phase transition to the radiation energy density of the Universe, $\rho_{\text{rad}} = g_* \pi^2 T^4 / 30$, given by

$$\alpha_* = \frac{\epsilon_*}{\rho_{\text{rad}}}, \quad (25)$$

with

$$\epsilon_* = \left[\Delta V_{\text{tot}} - \frac{T}{4} \frac{\partial \Delta V_{\text{tot}}}{\partial T} \right] \bigg|_{T=T_*}, \quad (26)$$

where $\Delta V_{\text{tot}} \equiv V_{\text{tot}}(\phi_{\text{false}}, T) - V_{\text{tot}}(\phi_{\text{true}}, T)$ is the free energy difference between the false and true vacuum. ϵ_* is related to the change in the trace of the energy-momentum tensor across the bubble wall [11,44]. The amplitude of GWs is also dictated by the duration of the FOPT, denoted by the parameter β, defined as [10]

$$\frac{\beta}{\mathbf{H}(T)} \simeq T \frac{d}{dT} \left(\frac{S_3}{T} \right). \quad (27)$$

Here, α_* and $\beta/\mathbf{H}(T)$ are evaluated at $T = T_*$. While S_3 can be evaluated using Eq. (20), the effective potential at sufficiently low temperatures, i.e., $T \ll M$ can be safely approximated as

$$V_{\text{tot}} \simeq \frac{g_D^2(t')}{2} T^2 \phi^2 + \frac{\lambda_{\text{eff}}(t')}{4} \phi^4,$$

$$\lambda_{\text{eff}}(t') = 4\pi\alpha_\lambda(t') / \left(1 - \frac{b}{2\pi} \alpha_D(0) t' \right)^{a_2/b},$$

$$t' = \ln(T/M). \quad (28)$$

In such a scenario the action can be approximated to be [45]

$$S = \frac{S_3}{T} - 4 \ln(T/M),$$

$$\frac{S_3}{T} \simeq -9.45 \times \frac{g_D(t')}{\lambda_{\text{eff}}(t')}. \quad (29)$$

In our estimation for the gravitational-wave amplitude we have used the above expressions (28) and (29) in calculating α, β, and the percolation temperature T_p.

We note that the NANOGrav Collaboration has estimated the required FOPT parameters using the thin-shell approximation for bubble walls (envelope approximation) [46], the semianalytic approximation [47], and full lattice
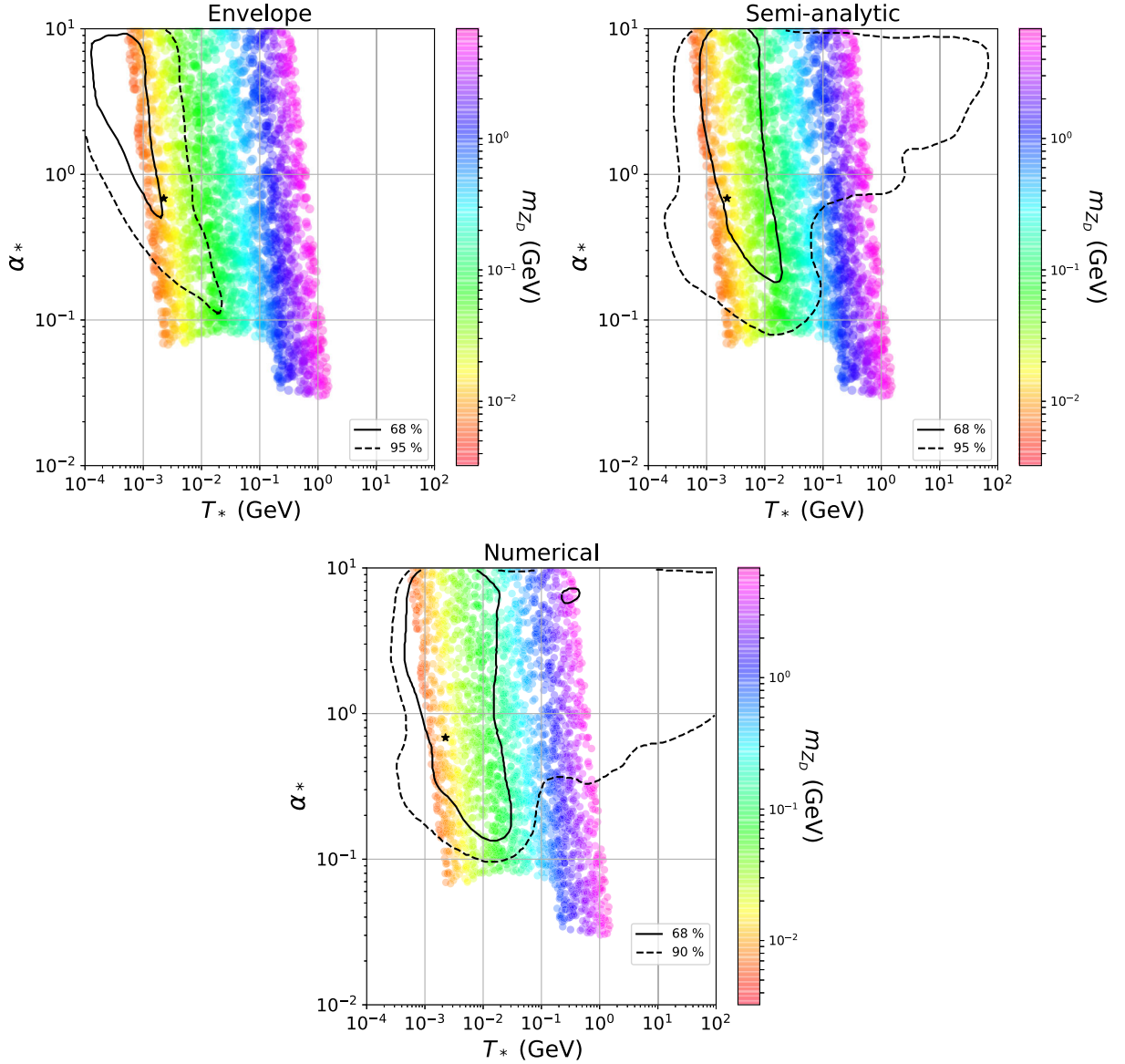
FIG. 2. Predictions for FOPT parameters in the α_*-T_* plane for our model. The gauge coupling g_D is varied in a range corresponding to $\alpha_D \in 0.002$–0.01. The contours correspond to the confidence levels obtained in Ref. [1] using the envelope approximation (left panel), semianalytic approximation (right panel), and numerical results (bottom panel).

results. Here we present the predictions of our model against the backdrop of their estimates in Fig. 2.

During a FOPT, there are three sources producing GWs: bubble collisions, the sound wave of the plasma, and the turbulence of the plasma [10,36,37,42,46,48]. These three contributions together give the resultant gravitational-wave power spectrum, given as [1]

$$\Omega_{\text{GW}}(f) = \Omega_\phi(f) + \Omega_{\text{sw}}(f) + \Omega_{\text{turb}}(f). \quad (30)$$

In general, each contribution has its own peak frequency and each GW spectrum can be parametrized in the following way [1]:

$$h^2\Omega(f) = \mathcal{R}\Delta(v_w)\left(\frac{\kappa\alpha_*}{1+\alpha_*}\right)^p\left(\frac{\mathbf{H}_*}{\beta}\right)^* \mathcal{S}(f/f_*^0), \quad (31)$$

where the prefactor $\mathcal{R} \simeq 7.69 \times 10^{-5} g_*^{-1/3}$ takes into account the redshift of the GW energy density, $\mathcal{S}(f/f_*^0)$ parametrizes the shape of the spectrum, and $\Delta(v_w)$ is the normalization factor which depends on the bubble wall velocity v_w. The Hubble parameter at $T = T_*$ is denoted by $\mathbf{H}_*$. Finally, the peak frequency today, f_*^0, is related to the value of the peak frequency at the time of emission, f_*, as follows:

$$f_*^0 \simeq 1.13 \times 10^{-10} \, \text{Hz} \left(\frac{f_*}{\beta}\right)\left(\frac{\beta}{\mathbf{H}_*}\right)\left(\frac{T_*}{\text{MeV}}\right)\left(\frac{g_*}{10}\right)^{1/6}, \quad (32)$$
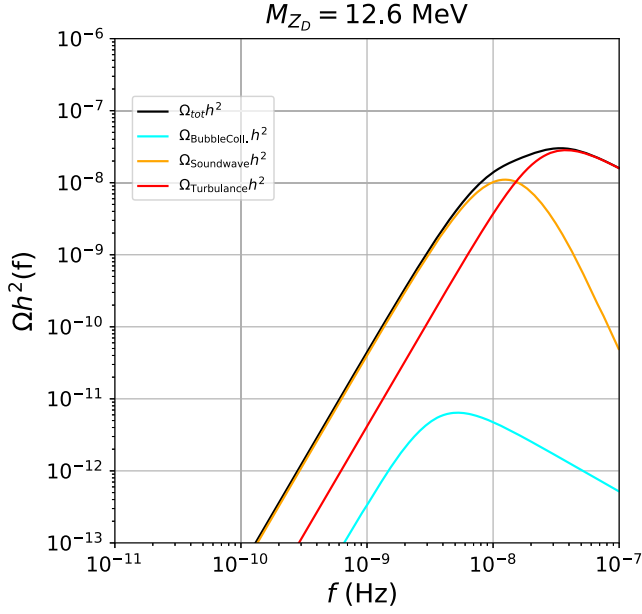
FIG. 3. GW spectrum $\Omega h^2(f)$ in terms of f for a FOPT with benchmark parameters $\alpha_* = 0.68$, $T_* = 2.25$ MeV, $g_D = 0.32$, $M_{Z_D} = 12.6$ MeV. The red, orange, cyan, and black curves correspond to the individual contributions from the turbulence of the plasma, sound wave of the plasma, bubble collisions, and the total contribution, respectively.

where g_* denotes the number of relativistic degrees of freedom at the time of the phase transition. The values of the peak frequency at the time of emission, the normalization factor, the spectral shape, and the exponents p and q are given in Table I of Ref. [1]. As for the efficiency factors, κ_ϕ was discussed in Refs. [12,28] and κ_{sw} is taken from Refs. [44,49]. On the other hand, the remaining efficiency factor κ_{turb} is taken to be approximately $0.1 \times \kappa_{sw}$ [1]. The bubble wall velocities were given in Refs. [50–54].

Based on the formulas presented above and by choosing a benchmark choice of model as well as FOPT parameters shown in Table I consistent with NANOGrav data at 95% C.L., we calculate the individual contributions to the GW energy density spectrum $\Omega h^2(f)$ from bubble collisions, the sound wave of the plasma, and the turbulence of the plasma, as well as the total contribution to $\Omega h^2(f)$. In Fig. 3, the red, orange, cyan, and black curves correspond to the individual contributions from the turbulence of the plasma, sound wave of the plasma, bubble collisions, and the total contribution to $\Omega h^2(f)$,

TABLE II. New particles for a radiative seesaw for neutrino mass with $U(1)_D$ symmetry.

	χ_1	Φ	$\Psi_{L,R}$	χ_2	η
$SU(2)_L$	1	1	1	2	1
$U(1)_D$	1	2	1	1	0

respectively. Due to the small value of the FOPT strength parameter α_*, as anticipated from earlier studies [55,56], the contribution from bubble collision is suppressed, as can be seen in Fig. 3.

V. NEUTRINO MASS

A dark Abelian gauge extension of SM can also be related to the origin of neutrino mass. Neutrino oscillation data suggest tiny but nonvanishing light neutrino masses with two large mixing [57]. Since nonzero neutrino mass and mixing cannot be explained in the SM, there have been several beyond-the-standard-model proposals. It turns out that the simplest $U(1)_D$ extension like the one discussed above augmented with additional discrete symmetries of fields can explain the origin of a light neutrino mass. Here we briefly mention two such possibilities for the origin neutrino mass.

First, we discuss a radiative origin of light neutrino masses, a natural origin of a low-scale seesaw. In addition to the singlet scalar Φ and the dark fermion Ψ in the minimal model discussed above, we need an additional scalar doublet χ and a scalar singlet η to realize a radiative seesaw. The required field content and their charges under $U(1)_D$ are shown in Table II. The relevant terms of the leptonic Lagrangian are given by

$$-\mathcal{L} \supset Y_\nu \bar{L} \tilde{\chi}_2 \Psi_R + Y_L \Phi^\dagger \overline{(\Psi_L)^c} \Psi_L + Y_R \Phi^\dagger \overline{(\Psi_R)^c} \Psi_R + \text{H.c.}$$

(33)

The relevant part of the scalar potential is

$$V \supset (\lambda_1 \chi_2^\dagger H \chi_1^\dagger \Phi + \lambda_2 \chi_1 \chi_1 \Phi^\dagger \eta + \text{H.c.}).$$

(34)

The singlet scalar η, neutral under $U(1)_D$, is introduced in order to avoid terms in the Lagrangian breaking conformal invariance [58]. The $U(1)_D$ symmetry is broken by a nonzero VEV of Φ to a remnant Z_2 symmetry, under which $\Psi_{L,R}, \chi_1, \chi_2$ are odd while all other fields are even. While light neutrino masses can be realized at the one-loop level with these Z_2-odd particles going inside the loop, the lightest Z_2-odd particle can be a stable DM candidate. A possible one-loop diagram for light neutrino mass is shown in Fig. 4. Since Z_2-odd particles take part in the loop, the origin of light neutrino masses is similar to the scotogenic mechanism [59]. The contribution from the diagram shown in Fig. 4 can be estimated as

$$(m_\nu)_{ij} \simeq \frac{\lambda_1^2 \langle H \rangle^2 \lambda_2 \langle \Phi \rangle^3 \langle \eta \rangle}{64\sqrt{2}\pi^2} \frac{(Y_\nu)_{ik}(M_\Psi)_k(Y_\nu^T)_{kj}}{M_{\chi_2}^6} I_\nu(r_{\chi_1}, r_k),$$

(35)

where $(M_\Psi)_k$ is the mass of pseudo-Dirac fermion states going inside the loop and I_ν is the corresponding loop
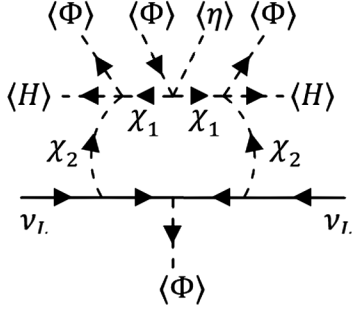
FIG. 4.   One loop origin of light neutrino masses.

function written in terms of $r_{\chi_1} = M_{\chi_1}^2/M_{\chi_2}^2$ and $r_k = M_{\Psi_k}^2/M_{\chi_2}^2$, with $M_{\chi_1}^2 = (m_{\chi_{r1}}^2 + m_{\chi_{i1}}^2)/2$ and $M_{\chi_2}^2 = (m_{\chi_{r2}}^2 + m_{\chi_{i2}}^2)/2$. The use of r, i in the subscripts denotes real and imaginary neutral parts of the corresponding complex scalar fields.

We now consider the realization of another low-scale seesaw, namely, an inverse seesaw with $U(1)_D$ symmetry. It turns out that a minimal $U(1)_D$ gauge symmetry is not sufficient to ensure the required structure of the inverse seesaw mass matrix. To have a minimal possibility we consider an additional Z_4 discrete symmetry. The new fields and their transformations under the imposed symmetries are shown in Table III. The relevant part of the Yukawa Lagrangian is

$$-\mathcal{L} \supset Y_\nu \bar{L} \tilde{H}_2 N_R + Y_{NS} N_R S_R \chi^\dagger + Y_S S_R S_R \Phi + \text{H.c.} \tag{36}$$

Clearly, the lepton-number-violating term involves Φ which also breaks the $U(1)_D$ symmetry. Therefore, a low-scale $U(1)_D$ naturally leads to a tiny lepton-number-violating term in the inverse seesaw mass matrix. After symmetry breaking, the light neutrino mass is given by

$$m_\nu \simeq \left(\frac{Y_\nu^T \langle H_2 \rangle}{\sqrt{2}}\right) \frac{1}{M_{NS}} \left(\frac{Y_S \langle \Phi \rangle}{\sqrt{2}}\right) \frac{1}{M_{NS}} \left(\frac{Y_\nu \langle H_2 \rangle}{\sqrt{2}}\right), \tag{37}$$

where $M_{NS} = \frac{Y_{NS}\langle\chi\rangle}{\sqrt{2}}$.

Thus, in both of the examples discussed here, the low-scale $U(1)_D$ symmetry can play a nontrivial role in light neutrino mass generation even though all of the SM fields are neutral under this symmetry.

TABLE III.   New particles for an inverse seesaw of neutrino mass with $U(1)_D$ symmetry.

	N_R	S_R	χ	Φ	H_2
$SU(2)_L$	1	1	1	1	2
$U(1)_D$	1	-1	0	2	1
Z_4	1	i	i	-1	1

VI. DARK MATTER AND COSMOLOGICAL CONSTRAINTS

Evidences from astrophysics and cosmology suggest the presence of a nonbaryonic form of matter giving rise to approximately 26% of the present Universe's energy density [57]. The simplest possibility is to consider a vector-like fermion Ψ having charge n_ψ under $U(1)_D$. Depending on the strength of gauge interactions, the relic abundance of DM can be realized either via thermal or nonthermal mechanisms. While the $U(1)_D$ gauge coupling was kept large in the analysis for FOPT and GWs above, DM interactions with the SM can still be suppressed due to small kinetic mixing between $U(1)_D$ and $U(1)_Y$. However, in the discussion on neutrino mass, we have introduced additional fields charged under both SM and $U(1)_D$ gauge symmetries. This will keep the one-loop kinetic mixing between $U(1)_D$ and $U(1)_Y$ suppressed but still large enough to produce Z_D in equilibrium. Thus, a light gauge boson with not too small kinetic mixing with $U(1)_Y$ can decay into SM leptons at late epochs [compared to the neutrino decoupling temperature $T_{\text{dec}}^\nu \sim \mathcal{O}(\text{MeV})$], increasing the effective relativistic degrees of freedom, which is tightly constrained by Planck 2018 data as $N_{\text{eff}} = 2.99_{-0.33}^{+0.34}$ [60]. Such constraints can be satisfied if $M_{Z_D} \gtrsim \mathcal{O}(10\text{ MeV})$ [61,62] which agrees with the benchmark value chosen in our FOPT and GW analysis. On the other hand, taking M_{Z_D} to a much higher regime will not explain the NANOGrav data. Therefore, we keep its benchmark at the minimum allowed value. A similar bound also exists for thermal DM masses in this regime which can annihilate into leptons. As shown in Ref. [63], such constraints from big bang nucleosynthesis as well as cosmic microwave background (CMB) measurements can be satisfied if $M_{\text{DM}} \gtrsim \mathcal{O}(1\text{ MeV})$. On the other hand, constraints from CMB measurements disfavor such light sub-GeV thermal DM production in the early Universe through s-channel annihilations into SM fermions [60]. Since fermion singlet DM in our model primarily annihilates via s-channel annihilations mediated by Z_D only, cosmological constraints are severe for a thermal DM mass around or below 10 MeV.

Due to the tight cosmological constraints on thermal DM with mass below 10 MeV as discussed above, we consider a nonthermal DM scenario, also known as the feebly interacting massive particle (FIMP) paradigm [64]. While we cannot make g_D very small, in order to satisfy the FOPT and GW criteria we choose the $U(1)_D$ charge of DM n_ψ to be very small.[2] For a DM mass above Z_D, it can be produced in the early Universe via annihilation of SM bath particles into DM, mediated by Z_D. In the left panel of Fig. 5 we

---

[2]FIMP DM in a similar Abelian gauge model with tiny $U(1)$ charge of DM was studied in earlier works like, for example, Ref. [65], where the authors studied $L_\mu - L_\tau$ gauge symmetry.
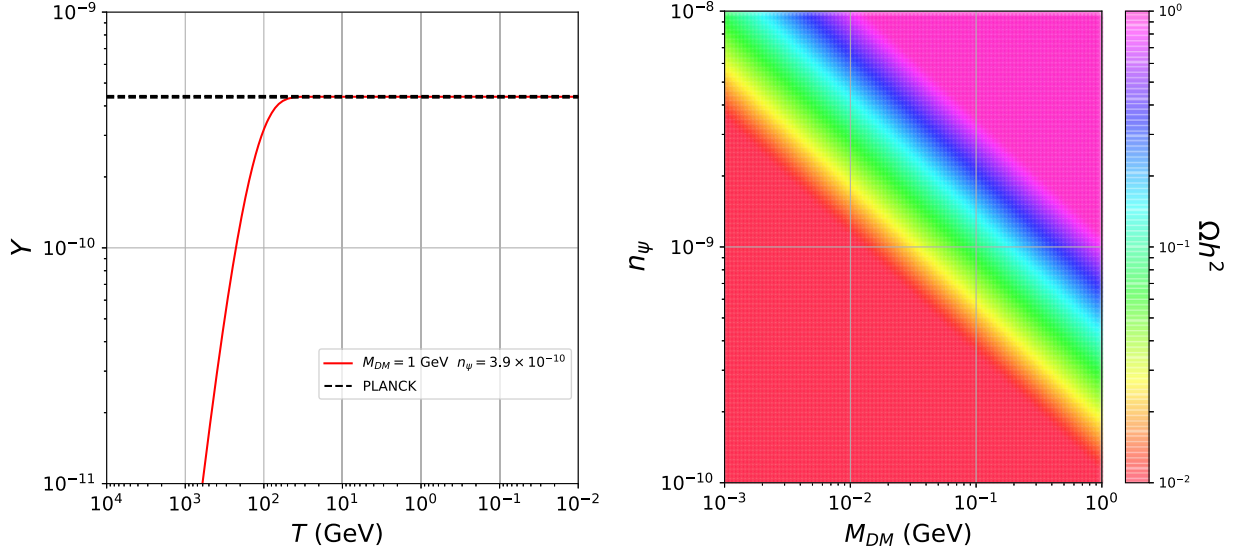
FIG. 5.   Left: comoving DM number density Y vs T for DM mass $M_{DM} = 1$ GeV and its $U(1)_D$ charge $n_\psi = 3.9 \times 10^{-10}$. Right: regions of $M_{DM} - n_\psi$ parameter space giving rise to the correct DM relic density for $g_D = 0.32$, $M_{Z_D} = 12.6$ MeV.

show the evolution of the comoving DM number density Y for DM mass $M_{DM} = 1$ GeV and its $U(1)_D$ charge $n_\psi = 3.9 \times 10^{-10}$. The kinetic mixing of Z_D with $U(1)_Y$ of the SM is taken to be approximately $\epsilon \sim g_D g'/(16\pi^2)$, similar to one-loop mixing. Clearly, DM with negligible initial abundance freezes in and gets saturated at lower temperatures, giving rise to the required relic density. In the right panel of Fig. 5 we show the parameter space in terms of $M_{DM} - n_\psi$ giving rise to the correct DM relic density while keeping the $U(1)_D$ sector parameters fixed at $g_D = 0.32$ and $M_{Z_D} = 12.6$ MeV. Since the DM mass is varied all the way up to 1 MeV for the right-panel plot of Fig. 5, which is below the Z_D mass threshold, we consider both annihilation and decay contributions to the DM relic density. Clearly, smaller values of n_ψ require a larger DM mass to satisfy the relic criteria. This is because smaller DM coupling leads to smaller nonthermal abundance, and hence a larger mass is required to generate the observed relic abundance. While we skip other phenomenological signatures of such DM, such sub-GeV DM can have very interesting phenomenology in the context of the latest experiments like XENON1T [66], as has been discussed in Refs. [67–70] among others. Such Dirac fermion DM, upon receiving a tiny Majorana mass contribution from the singlet scalar (as discussed above in the context of radiative neutrino mass) can give rise to inelastic DM [71,72] with interesting DM phenomenology [73].

VII. CONCLUSION

Motivated by the NANOGrav Collaboration's recent analysis of their 12.5 yr data implying a possible origin of a stochastic GW spectrum from a first-order phase transition below the EW scale, we revisited the simplest possibility of a dark Abelian gauge extension of the SM. While the SM fields are neutral under this gauge symmetry, a complex scalar singlet with nonvanishing gauge charge can lead to the necessary symmetry breaking. We further considered a classical conformal invariance such that the symmetry breaking occurs through radiative corrections to the scalar potential, keeping the model minimal. While additional dark fermions can be introduced in order to explain the origin of dark matter, for the details of the phase transition we confined ourselves to only the singlet scalar–vector boson interactions, ignoring other scalar portal or Yukawa interactions for simplicity. We performed a numerical scan to show how a light gauge boson Z_D at the sub-GeV scale can explain the FOPT parameters given in Ref. [1] in order to explain their data. We also commented on the possibility of connecting such $U(1)_D$ models to light neutrino mass and dark matter in a common setup. Due to tight cosmological constraints on such a light vector boson Z_D as well as DM whose interactions with the SM sector are mediated by Z_D via kinetic mixing, we considered a nonthermal DM scenario. By choosing $U(1)_D$ sector parameters in a way that satisfies NANOGrav data, we performed a numerical scan over DM mass in the sub-GeV range and its $U(1)_D$ charge that can give rise to the correct nonthermal DM relic.

Due to the complementary nature of the observable signatures of such minimal models, especially in the context of GWs from FOPT as well as typical sub-GeV dark matter signatures, near-future experiments should be able to scrutinize such predictive scenarios. Additionally,

while PTAs like NANOGrav offer a complementary GW window to proposed space-based interferometers, more data are needed to confirm whether this is a clear detection of GWs and whether it is due to FOPT or astrophysical sources like SMBHB mergers (possible ways of distinguishing cosmological backgrounds from astrophysical foregrounds have been discussed recently in Ref. [74]).

[1] Z. Arzoumanian *et al.* (NANOGrav Collaboration), arXiv: 2104.13930.

[2] Z. Arzoumanian *et al.* (NANOGrav Collaboration), Astrophys. J. Lett. **905,** L34 (2020).

[3] S. Blasi, V. Brdar, and K. Schmitz, Phys. Rev. Lett. **126,** 041305 (2021).

[4] J. Ellis and M. Lewicki, Phys. Rev. Lett. **126,** 041304 (2021).

[5] L. Bian, R. G. Cai, J. Liu, X. Y. Yang, and R. Zhou, Phys. Rev. D **103,** L081301 (2021).

[6] W. Ratzinger and P. Schwaller, SciPost Phys. **10,** 047 (2021).

[7] A. Addazi, Y. F. Cai, Q. Gan, A. Marciano, and K. Zeng, Sci. China Phys. Mech. Astron. **64,** 290411 (2021).

[8] Y. Nakai, M. Suzuki, F. Takahashi, and M. Yamada, Phys. Lett. B **816,** 136238 (2021).

[9] R. Zhou, L. Bian, and J. Shu, arXiv:2104.03519.

[10] C. Caprini, M. Hindmarsh, S. Huber, T. Konstandin, J. Kozaczuk, G. Nardini, J. M. No, A. Petiteau, P. Schwaller, G. Servant *et al.*, J. Cosmol. Astropart. Phys. 04 (2016) 001.

[11] C. Caprini, M. Chala, G. C. Dorsch, M. Hindmarsh, S. J. Huber, T. Konstandin, J. Kozaczuk, G. Nardini, J. M. No, K. Rummukainen *et al.*, J. Cosmol. Astropart. Phys. 03 (2020) 024.

[12] R. Jinno and M. Takimoto, Phys. Rev. D **95,** 015020 (2017).

[13] A. Mohamadnejad, Eur. Phys. J. C **80,** 197 (2020).

[14] Y. G. Kim, K. Y. Lee, and S. H. Nam, Phys. Rev. D **100,** 075038 (2019).

[15] T. Hasegawa, N. Okada, and O. Seto, Phys. Rev. D **99,** 095039 (2019).

[16] C. Marzo, L. Marzola, and V. Vaskonen, Eur. Phys. J. C **79,** 601 (2019).

[17] K. Hashino, M. Kakizaki, S. Kanemura, P. Ko, and T. Matsui, J. High Energy Phys. 06 (2018) 088.

[18] C. W. Chiang and E. Senaha, Phys. Lett. B **774,** 489 (2017).

[19] L. Dolan and R. Jackiw, Phys. Rev. D **9,** 3320 (1974).

[20] M. Quiros, arXiv:hep-ph/9901312.

[21] P. Fendley, Phys. Lett. B **196,** 175 (1987).

[22] R. R. Parwani, Phys. Rev. D **45,** 4695 (1992); **48,** 5965(E) (1993).

[23] P. B. Arnold and O. Espinosa, Phys. Rev. D **47,** 3546 (1993); **50,** 6662(E) (1994).

[24] A. Mazumdar and G. White, Rep. Prog. Phys. **82,** 076901 (2019).

[25] M. B. Hindmarsh, M. Lüben, J. Lumma, and M. Pauly, SciPost Phys. Lect. Notes **24,** 1 (2021).

[26] A. D. Linde, Phys. Lett. **100B,** 37 (1981).

[27] J. Ellis, M. Lewicki, and J. M. No, J. Cosmol. Astropart. Phys. 04 (2019) 003.

[28] J. Ellis, M. Lewicki, and V. Vaskonen, J. Cosmol. Astropart. Phys. 11 (2020) 020.

[29] M. S. Turner and F. Wilczek, Phys. Rev. Lett. **65,** 3080 (1990).

[30] A. Kosowsky, M. S. Turner, and R. Watkins, Phys. Rev. D **45,** 4514 (1992).

[31] A. Kosowsky, M. S. Turner, and R. Watkins, Phys. Rev. Lett. **69,** 2026 (1992).

[32] A. Kosowsky and M. S. Turner, Phys. Rev. D **47,** 4372 (1993).

[33] M. S. Turner, E. J. Weinberg, and L. M. Widrow, Phys. Rev. D **46,** 2384 (1992).

[34] M. Hindmarsh, S. J. Huber, K. Rummukainen, and D. J. Weir, Phys. Rev. Lett. **112,** 041301 (2014).

[35] J. T. Giblin and J. B. Mertens, Phys. Rev. D **90,** 023532 (2014).

[36] M. Hindmarsh, S. J. Huber, K. Rummukainen, and D. J. Weir, Phys. Rev. D **92,** 123009 (2015).

[37] M. Hindmarsh, S. J. Huber, K. Rummukainen, and D. J. Weir, Phys. Rev. D **96,** 103520 (2017); **101,** 089902(E) (2020).

[38] M. Kamionkowski, A. Kosowsky, and M. S. Turner, Phys. Rev. D **49,** 2837 (1994).

[39] A. Kosowsky, A. Mack, and T. Kahniashvili, Phys. Rev. D **66,** 024030 (2002).

[40] C. Caprini and R. Durrer, Phys. Rev. D **74,** 063521 (2006).

[41] G. Gogoberidze, T. Kahniashvili, and A. Kosowsky, Phys. Rev. D **76,** 083002 (2007).

[42] C. Caprini, R. Durrer, and G. Servant, J. Cosmol. Astropart. Phys. 12 (2009) 024.

[43] P. Niksa, M. Schlederer, and G. Sigl, Classical Quantum Gravity **35,** 144001 (2018).

[44] D. Borah, A. Dasgupta, K. Fujikura, S. K. Kang, and D. Mahanta, J. Cosmol. Astropart. Phys. 08 (2020) 046.

[45] A. D. Linde, Nucl. Phys. **B216,** 421 (1983); **B223,** 544(E) (1983).

[46] R. Jinno and M. Takimoto, Phys. Rev. D **95,** 024009 (2017).

[47] M. Lewicki and V. Vaskonen, Eur. Phys. J. C **81,** 437 (2021).

[48] P. Binetruy, A. Bohe, C. Caprini, and J. F. Dufaux, J. Cosmol. Astropart. Phys. 06 (2012) 027.

[49] J. R. Espinosa, T. Konstandin, J. M. No, and G. Servant, J. Cosmol. Astropart. Phys. 06 (2010) 028.

[50] P. J. Steinhardt, Phys. Rev. D **25**, 2074 (1982).

[51] S. J. Huber and M. Sopena, arXiv:1302.1044.

[52] L. Leitao and A. Megevand, Nucl. Phys. **B891**, 159 (2015).

[53] G. C. Dorsch, S. J. Huber, and T. Konstandin, J. Cosmol. Astropart. Phys. 12 (2018) 034.

[54] J. M. Cline and K. Kainulainen, Phys. Rev. D **101**, 063525 (2020).

[55] D. Bodeker and G. D. Moore, J. Cosmol. Astropart. Phys. 05 (2017) 025.

[56] J. Ellis, M. Lewicki, J. M. No, and V. Vaskonen, J. Cosmol. Astropart. Phys. 06 (2019) 024.

[57] P. A. Zyla et al. (Particle Data Group), Prog. Theor. Exp. Phys. **2020**, 083C01 (2020).

[58] A. Ahriche, K. L. McDonald, and S. Nasri, J. High Energy Phys. 06 (2016) 182.

[59] E. Ma, Phys. Rev. D **73**, 077301 (2006).

[60] N. Aghanim et al. (Planck Collaboration), Astron. Astrophys. **641**, A6 (2020).

[61] M. Ibe, S. Kobayashi, Y. Nakayama, and S. Shirai, J. High Energy Phys. 04 (2020) 009.

[62] M. Escudero, D. Hooper, G. Krnjaic, and M. Pierre, J. High Energy Phys. 03 (2019) 071.

[63] N. Sabti, J. Alvey, M. Escudero, M. Fairbairn, and D. Blas, J. Cosmol. Astropart. Phys. 01 (2020) 004.

[64] L. J. Hall, K. Jedamzik, J. March-Russell, and S. M. West, J. High Energy Phys. 03 (2010) 080.

[65] See for example, A. Biswas, S. Choubey, and S. Khan, J. High Energy Phys. 02 (2017) 123.

[66] E. Aprile et al. (XENON Collaboration), Phys. Rev. D **102**, 072004 (2020).

[67] D. Borah, S. Mahapatra, and N. Sahu, Nucl. Phys. **B968**, 115407 (2021).

[68] D. Borah, S. Mahapatra, D. Nanda, and N. Sahu, Phys. Lett. B **811**, 135933 (2020).

[69] M. Dutta, S. Mahapatra, D. Borah, and N. Sahu, Phys. Rev. D **103**, 095018 (2021).

[70] D. Borah, M. Dutta, S. Mahapatra, and N. Sahu, arXiv:2104.05656.

[71] D. Tucker-Smith and N. Weiner, Phys. Rev. D **64**, 043502 (2001).

[72] Y. Cui, D. E. Morrissey, D. Poland, and L. Randall, J. High Energy Phys. 05 (2009) 076.

[73] N. Song, S. Nagorny, and A. C. Vincent, arXiv:2104.09517.

[74] C. J. Moore and A. Vecchio, arXiv:2104.15130.